*J. S. Afr. Inst. Min. Metall.*, vol. 86, no. 6.
Jun. 1986. pp. 195-204.

# The protection of vertical shafts by pillars in shallow and moderately deep hard-rock mines

by S. BUDAVARI*

**SYNOPSIS**

The effects of shaft pillars left in deep-level hard-rock mines during the extraction of tabular deposits were studied some time ago, resulting in the formulation of design principles and procedures, which have been used with success in the design of shaft pillars in the deep-level gold mines of South Africa. The method has not yet been utilized in the design of shaft pillars in shallow and moderately deep hard-rock mines. The purpose of the present study was to remedy the situation since a great number of deposits are worked at those depths.

The object of this paper is to present governing equations for the components of stress and differential movement as derived by use of an elastic model. The pillar is taken to be circular in the plane of a horizontal deposit. On the basis of the numerical results obtained, a study was made of the distribution of the vertical strain and tilt along the axis of the shaft, and of the vertical stress along the shaft and across the pillar. In every case investigated, the most adverse geometry was taken into consideration.

By use of an empirical criterion and the results of some *in situ* observations, the determination of pillar dimensions and differential displacement components for South African gold-mining conditions is demonstrated. Pillar dimensions for shallow and moderate depths are compared with those accepted for deep-level conditions.

**SAMEVATTING**

Die uitwerking van skagpilare wat tydens die uitmyning van tafelvormige afsettings in diepharderotsmyne agtergelaat is, is 'n tyd gelede bestudeer en dit het gelei tot die formulering van ontwerpbeginsels en -prosedures wat suksesvol toegepas is by die ontwerp van skagpilare in die diepgoudmyne van Suid-Afrika. Die metode is nog nie vir die ontwerp van skagpilare in vlak en matig diep harderotsmyne gebruik nie. Die doel van die huidige studie was om daardie toedrag van sake te verhelp, aangesien baie afsettings op daardie dieptes ontgin word.

Die doel van hierdie referaat is om die bepalende vergelykings vir die spannings- en differensiaalbewegingskomponente, soos met gebruik van 'n elastiese model afgelei, aan te gee. Die pilaar word as sirkelvormig in die vlak van 'n horisontale afsetting beskou. Op grond van die numeriese resultate wat verkry is, is daar 'n studie van die verdeling van die vertikale vervorming en kanteling langs die as van die skag, en van die vertikale spanning langs die skag en oor die pilaar gemaak. Die nadeligste geometrie is in elke geval wat ondersoek is, in aanmerking geneem.

Die bepaling van die pilaarafmetings en komponente van die differensiaalverplasing vir Suid-Afrikaanse goudmyntoestande word met gebruik van 'n empiriese maatstaf, en die resultate van sommige waarnemings ter plaatse, gedemonstreer. Die pilaarafmetings vir vlak en matige dieptes word vergelyk met dié wat vir diepmyntoestande aanvaar word.

## Introduction

An analytical method for the protection of vertical shafts from the mining of narrow tabular orebodies in their vicinities was recorded by Salamon[1] in 1964. Daemen[2] used Salamon's approach to analyse the effects of protective pillars on shafts serving mining operations at shallow and moderate depths. Two further publications[3,4] gave details of the design of shaft pillars in deep-level hard-rock mines. The practical approach and the design principles evolved from the application of this method have not yet been utilized in the design of shaft pillars in shallow and moderately deep mines, and it is the purpose of the present paper to redress this situation.

The shaft pillar formed when a horizontal reef is left unmined in an area surrounding the shaft is considered to be circular. The rock mass affected is assumed to behave as a homogeneous, linearly elastic substance. The effective stoping width is taken to be uniform and small compared with the depth of the deposit.

Since the distributions of the components of vertical stress and differential movement along the axis of the shaft have practical significance, they are determined and analysed for the conditions specified. For comparative purposes, stresses across the shaft pillar are also studied. The magnitudes of both stress and differential movement are evaluated for the most adverse geometries. However, the surface effects of shaft pillars are not considered.

## Derivation of Stress and Displacement Components

In the determination of the effects of an excavation on the surrounding rock mass, the mined-out area is divided into elemental areas referred to as face elements. Each face element is associated with a certain magnitude of convergence. This convergence component induces elemental displacements of varying magnitudes at every point in the affected rock mass. The convergence component associated with another face element also induces elemental displacements at the same points. The total induced effects at an arbitrary point in the rock are the sums of the corresponding elemental displacement components due to the convergence components associated with all the face elements in the area of influence.

The contribution of a face element to the total induced effects at a point depends on the position of the element relative to the point and on the magnitude of the associated convergence component. It is also dependent on the mechanical properties of the medium purporting to model the behaviour of the rock mass involved.

* Professor of Rock Mechanics, Department of Mining Engineering, University of the Witwatersrand, 1 Jan Smuts Avenue, Johannesburg 2001.

 SA ISSN 0038-223X/ $3.00 + 0.00. Paper received 7th January, 1986.

It can be seen from the preceding paragraphs that the induced displacements throughout the rock mass are determined by the distribution of convergence components on the plane of the excavation. A knowledge of certain mathematical operators is also essential. These operators, known as kernels, are used together with the convergence to determine the magnitude of the elemental displacement components as a function of the mechanical properties of the medium, and the spatial disposition of the face elements. Once the displacements have been determined, the strain component can be derived and, using the physical equations of the mathematical model, one can determine the induced stresses from the strain components.

*Elemental Displacement Components*

The elemental displacements induced at a point P in the solid rock with coordinates x, y, z, by the convergence $s_z(\xi, \eta)$ over the elemental area $\Delta A$ were defined by Salamon[5] as

$$\Delta u = -\frac{s_z(\xi, \eta)}{\pi}(\xi - x)\, F_2(r^2, z, H)\, \Delta A, \quad \ldots\ldots (1)$$

$$\Delta v = -\frac{s_z(\xi, \eta)}{\pi}(\eta - y)\, F_2(r^2, z, H)\, \Delta A, \quad \ldots\ldots (2)$$

$$\Delta w = -\frac{s_z(\xi, \eta)}{\pi} F_1(r^2, z, H)\, \Delta A, \quad \ldots\ldots\ldots (3)$$

where $r^2 = (\xi - x)^2 + (\eta - y)^2$. $\ldots\ldots\ldots (4)$

The relationships among the geometrical variables involved are depicted in Fig. 1. The origin of the x, y, and z coordinate system is located on the surface at the top of the shaft, and the z-axis is directed downwards along the centre line of the shaft. The functions $F_1$ and $F_2$ will be defined in the next subsection.

By use of the geometrical relations

$$(\xi - x) = r\cos\phi, \quad (\eta - y) = r\sin\phi, \quad \ldots\ldots\ldots (5)$$

the elemental displacement components can be expressed in cylindrical coordinates as

$$\Delta u = -\frac{s_z(r, \phi)}{\pi} r\cos\phi\, F_2\, \Delta A, \quad \ldots\ldots\ldots (6)$$

$$\Delta v = -\frac{s_z(r, \phi)}{\pi} r\sin\phi\, F_2\, \Delta A, \quad \ldots\ldots\ldots (7)$$

$$\Delta w = -\frac{s_z(r, \phi)}{\pi} F_1\, \Delta A. \quad \ldots\ldots\ldots (8)$$

*The Influence Functions*

The kernels $F_1$ and $F_2$ for a homogeneous, isotropic model and finite depth conditions consist of three components. The first component in each kernel is the basic function, which yields the elemental displacements for a face element at infinite depth. The other two components serve to eliminate the shearing and normal stress components respectively on the ground surface as required by the boundary conditions for the finite depth solution.

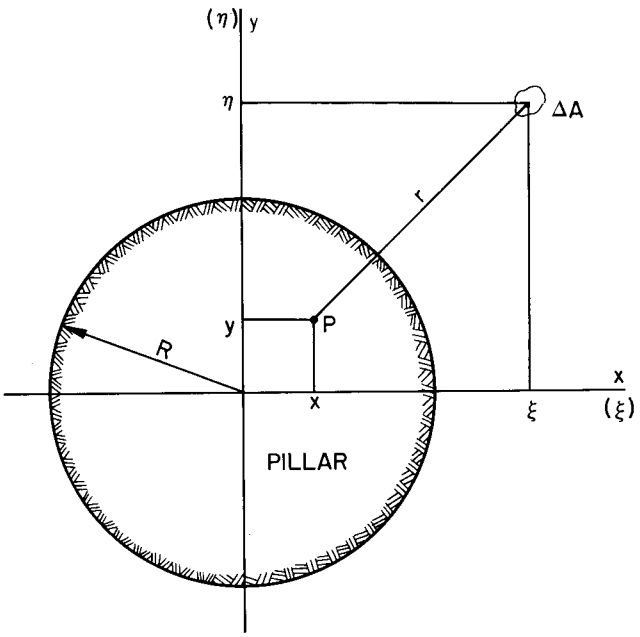


**Fig. 1—Coordinate system used in the study**

If the two kernels and their components are denoted by

$$F_1 = F_{11} + F_{12} + F_{13}, \quad \ldots\ldots\ldots (9)$$

$$F_2 = F_{21} + F_{22} + F_{23}, \quad \ldots\ldots\ldots (10)$$

then the various components as specified by Salamon can be written as

$$F_{11} = -\frac{z_1}{8(1-\nu)} \frac{2(2-\nu)z_1^2 + (1-2\nu)r^2}{(r^2 + z_1^2)^{5/2}}, \quad \ldots (11)$$

$$F_{12} = -\frac{z_2}{8(1-\nu)} \frac{2(2-\nu)z_2^2 + (1-2\nu)r^2}{(r^2 + z_2^2)^{5/2}}, \quad \ldots\ldots (12)$$

$$F_{13} = \frac{1}{4(1-\nu)}\left\{\frac{2(1-\nu)z_2}{(r^2 + z_2^2)^{3/2}} + [z + 2H(1-\nu)]\frac{2z_2^2 - r^2}{(r^2 + z_2^2)^{5/2}} + 3Hzz_2\frac{2z_2^2 - 3r^2}{(r^2 + z_2^2)^{7/2}}\right\}, \quad \ldots\ldots\ldots (13)$$

$$F_{21} = \frac{1}{8(1-\nu)} \frac{2(1+\nu)z_1^2 - (1-2\nu)r^2}{(r^2 + z_1^2)^{5/2}}, \quad \ldots\ldots\ldots (14)$$

$$F_{22} = \frac{1}{8(1-\nu)} \frac{2(1+\nu)z_2^2 - (1-2\nu)r^2}{(r^2 + z_2^2)^{5/2}}, \quad \ldots\ldots (15)$$

$$F_{23} = \frac{1}{4(1-\nu)}\left[\frac{(1-2\nu)}{(r^2 + z_2^2)^{3/2}} - \frac{3z_2(z_1 + 2\nu H)}{(r^2 + z_2^2)^{5/2}} + \frac{3Hz(4z_2^2 - r^2)}{(r^2 + z_2^2)^{7/2}}\right]. \quad \ldots\ldots (16)$$

In the above expressions

$$z_1 = z - H \text{ and } z_2 = z + H, \quad \ldots\ldots (17)$$

where $H$ is the depth of the horizontal reef below surface. The symbol $\nu$ represents Poisson's ratio.

*Induced Displacement Components*

Before the relevant displacement functions are derived, a simplification can be considered and introduced in the calculations. It concerns the convergence distribution. If one takes the convergence to be a constant value, $s_m$, over the entire worked-out area, the derivation of the appropriate distribution functions will be substantially simplified.

As indicated above, the total induced displacement components can be calculated by integration of the separate influences on P of all the face elements over the area of extraction $A$. The summation of the individual effects yields the following expressions for the total induced displacement components:

$$u = -\frac{s_m}{\pi}\iint_A F_2\, r\cos\phi\, \Delta A, \quad \ldots\ldots (18)$$

$$v = -\frac{s_m}{\pi}\iint_A F_2\, r\sin\phi\, \Delta A, \quad \ldots\ldots (19)$$

$$w = -\frac{s_m}{\pi}\iint_A F_1\, \Delta A \quad \ldots\ldots (20)$$

Substitution of the numerical expressions for $F_1$ and $F_2$ into equations (18) to (20) yields equations (A1) to (A3), which are given in the Addendum.

*Strain Components and Tilt*

On the basis of the strain–displacement relationships of the theory of elasticity, the induced strain components can be derived by the appropriate differentiation of the displacement functions. Thus, differentiating equation (18) with respect to $x$ and using expressions (4) and (5), one can write

$$\epsilon_x = \frac{\partial u}{\partial x} = -\frac{s_m}{\pi}\iint_A \left[\frac{\partial F_2}{\partial(r^2)}\frac{\partial(r^2)}{\partial x}(\xi - x) - F_2\right]\Delta A,$$

$$\epsilon_x = -\frac{s_m}{\pi}\iint_A \left[-\frac{\partial F_2}{\partial(r^2)}2(\xi - x)^2 - F_2\right]\Delta A,$$

$$\epsilon_x = \frac{s_m}{\pi}\iint_A \left[2r^2\cos^2\phi\frac{\partial F_2}{\partial(r^2)} + F_2\right]\Delta A. \quad \ldots\ldots (21)$$

The two other normal strain components can be derived similarly. The final equations are

$$\epsilon_y = \frac{s_m}{\pi}\iint_A \left[2r^2\sin^2\phi\frac{\partial F_2}{\partial(r^2)} + F_2\right]\Delta A, \quad \ldots\ldots (22)$$

$$\epsilon_z = -\frac{s_m}{\pi}\iint_A \frac{\partial F_1}{\partial z}\Delta A. \quad \ldots\ldots (23)$$

After the appropriate substitutions, the corresponding expressions for the normal strain components can be obtained. Since at this stage only the vertical strain component, $\epsilon_z$, has relevance to the study, its full expression is presented as equation (A4) in the Addendum.

Apart from the normal strain components introduced above, the tilt, $\partial u/\partial z$, is important from practical points of view. Therefore, its corresponding expressions are given in equations (24) and (A5):

$$t_x = \frac{\partial u}{\partial z} = -\frac{s_m}{\pi}\iint_A \frac{\partial F_2}{\partial z} r\cos\phi\, \Delta A. \quad \ldots\ldots (24)$$

*Vertical Stress Component*

The stress–strain relations for an isotropic linearly elastic solid allow one to write the following expression for the induced vertical stress component:

$$\sigma_z = \frac{E}{(1-\nu)}\left[\frac{\nu}{1-2\nu}(\epsilon_x + \epsilon_y + \epsilon_z) + \epsilon_z\right], \quad \ldots\ldots (25)$$

where $E$ is the modulus of elasticity.

On the substitution of expressions (21), (22), and (23) into (25), the equation for the vertical stress component is obtained:

$$\sigma_z = \frac{Es_m}{\pi(1+\nu)(1-2\nu)}\iint_A \left\{2\nu\left[F_2 + r^2\frac{\partial F_2}{\partial(r^2)}\right] - (1-\nu)\frac{\partial F_1}{\partial z}\right\}\Delta A. \quad \ldots\ldots (26)$$

The expanded form of this equation is given as (A6).

## Analysis of Differential Displacements

As indicated earlier, it was shown by Salamon[3] that the magnitudes of vertical strain and tilt that are induced along the axis of the shaft are sufficient to quantify the effects of a shaft pillar on the rock masses in which the shaft is excavated. In this section of the paper, the distributions of these differential displacement components are discussed.

*The Vertical Strain Component*

The distribution of vertical induced strain along the axis

of the shaft can be determined from equation (A4). The most adverse geometry for this differential displacement component is brought about when the reef is totally extracted outside the shaft pillar, as shown in Fig. 2(a). For this condition, the limits of the integration are $\phi = 0$ to $2\pi$ and $r = R$ to $\infty$, and the expression for the elemental area $\Delta A$ becomes $rd\phi dr$.

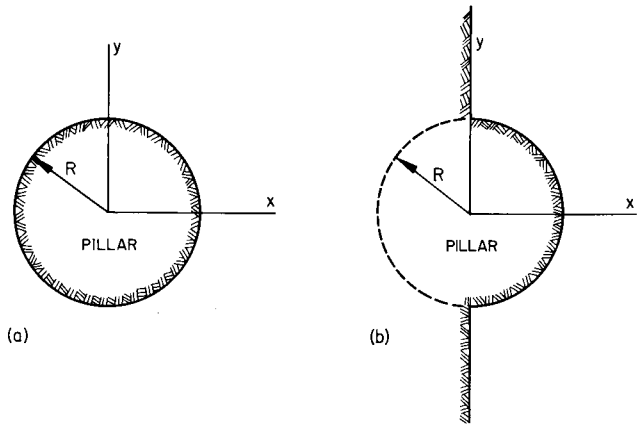


**Fig. 2—Most adverse geometries with respect to (a) vertical strain and stress, and (b) tilt**

In Fig. 3 the variations of $\epsilon_z$ along the shaft axis for three different cases are shown. The radii of the pillars were selected to yield approximately equal resultant stresses (100 MPa) at the pillar–shaft intersections. The relevant basic data are tabulated in Table I. For all three cases, Poisson's ratio and the stoping width were kept constant at 0,2 and 1 m, respectively. The data plotted in Fig. 3 were obtained by numerical integration.

TABLE I
STRESS AT PILLAR-SHAFT INTERSECTION

| Depth m | Pillar radius m | Resultant stress MPa |
|---|---|---|
| 150 | 110 | 97,7 |
| 300 | 160 | 100,7 |
| 600 | 210 | 99,1 |

The following can be deduced from Fig. 3. All the strains are positive, and therefore contractive. At shallow depths, the strain distributions are asymmetrical about the plane of the reef. With increasing values of $H/R$, they tend to become symmetrical. The largest values of the maximum strain are brought about in the footwall strata.

The analysis of additional data showed that the maximum values of vertical strain in the hanging- and footwalls were located close to $z_1/R = \mp 0,6$, respectively. The variation of normalized maximum strain as a function of $H/R$ is depicted in Fig. 4.

*Tilt along the Shaft Axis*

For the same values of pillar radius and depth as used in the preceding subsection, the distribution of induced tilt along the shaft axis was determined from equation

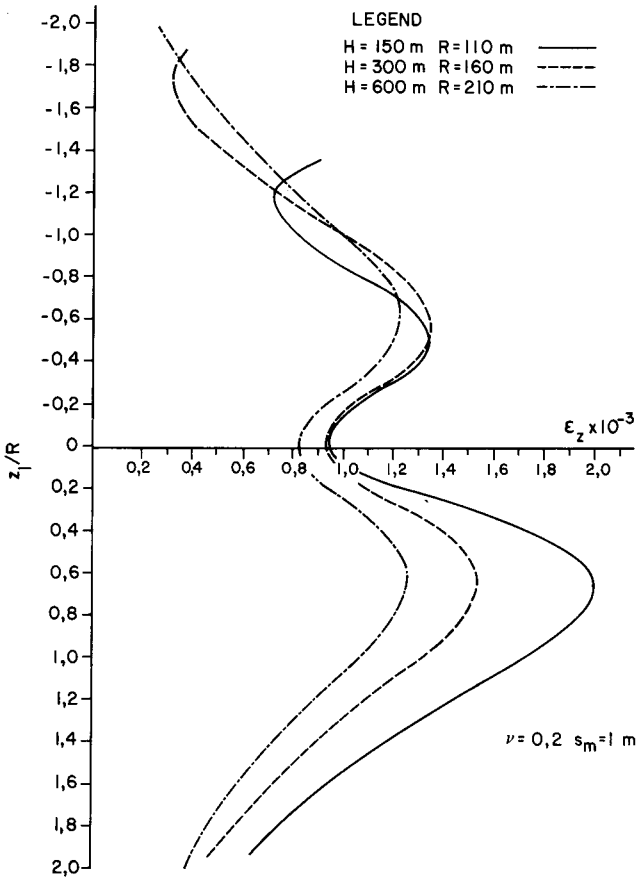


**Fig. 3—Distribution of vertical strain along the shaft**

(A5) and plotted in Fig. 5. The numerical integration was carried out within the limits of integration $\phi = -\pi/2$ to $\pi/2$ and $r = R$ to $\infty$. The geometrical interpretation of these limits is given in Fig. 2(b). Again, Poisson's ratio was taken to be 0,2.

As indicated in Fig. 5, the tilt in the hangingwall is positive, and its magnitude decreases with increasing values of $H/R$. Maximum tilt occurs at $z_1/R = -0,5$. The tilts in the footwall are mostly negative, and their absolute values are considerably smaller than the corresponding values in the hangingwall. The variation of maximum normalized tilt is shown in Fig. 4.

## Analysis of Vertical Stress Component

In the design of underground excavations in close proximity of a shaft, the resultant stresses acting in the rock masses play a dominant role. A knowledge of the magnitude and distribution of the vertical stress component along the shaft and across the pillar is essential.

*Vertical Stress along the Axis of the Shaft*

For the cases presented in Table I, the vertical stresses induced in the rock along the shaft were computed from equation (A6). The limits of integration and the most adverse geometry relevant to the case were the same as for the induced vertical strain. The material parameters used in the calculations, namely the modulus of elasticity and Poisson's ratio, were 72 GPa and 0,2 respectively. The results obtained are presented in Fig. 6.

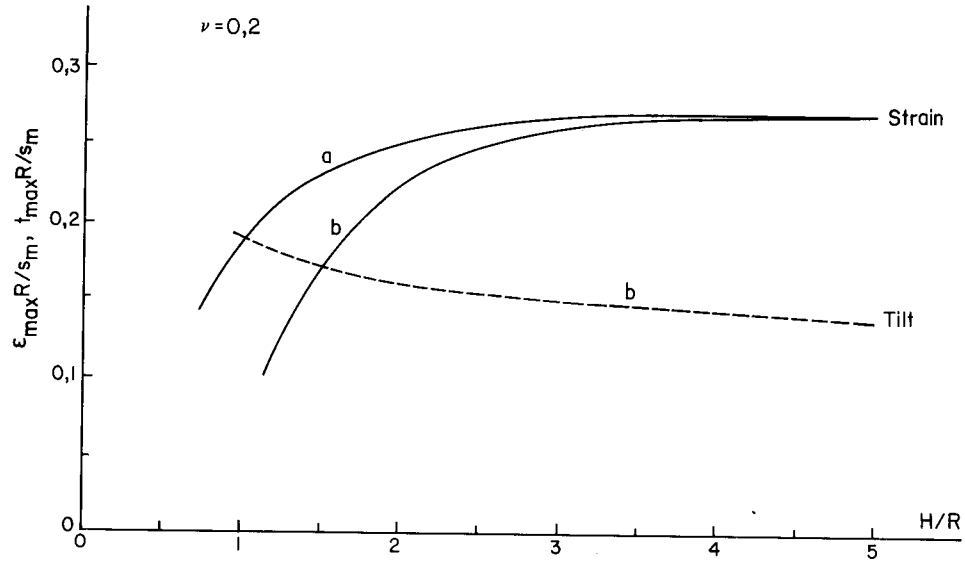


**Fig. 4—Maximum values of (a) normalized strain in footwall, and (b) strain and tilt in hangingwall**

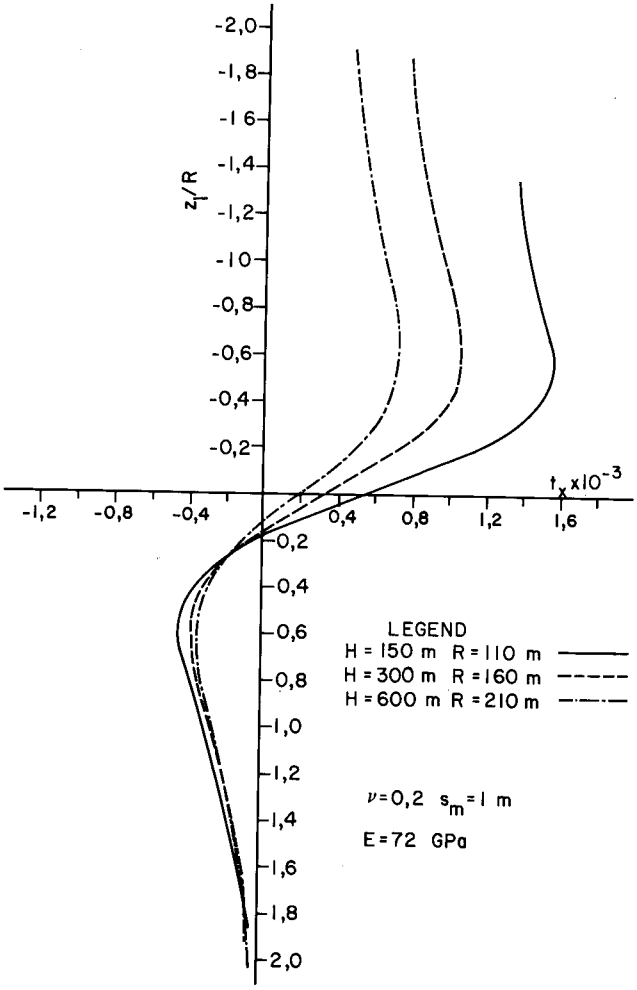


**Fig. 5—Distribution of tilt along the shaft**

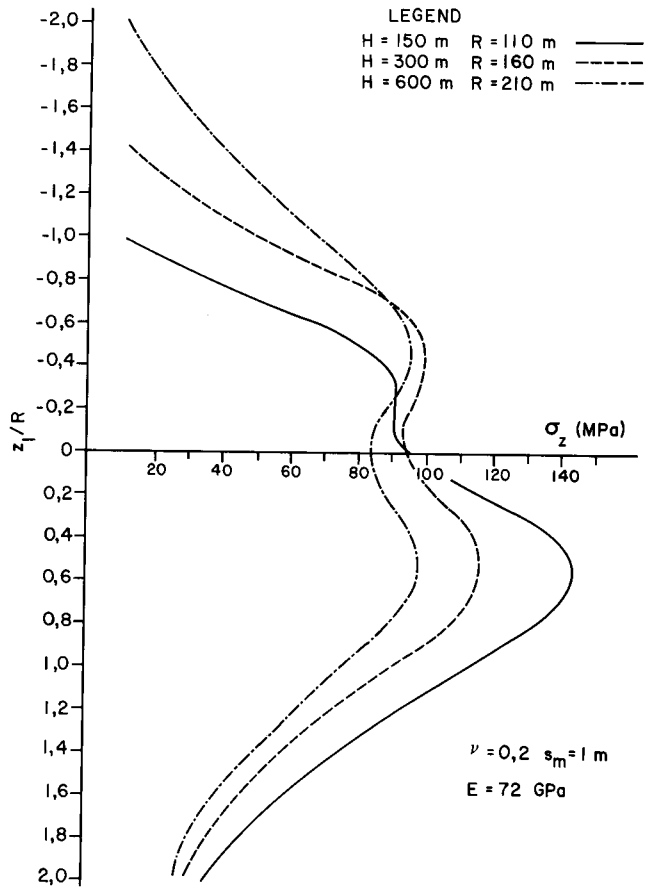


**Fig. 6—Distribution of induced vertical stress along the shaft**

It can be seen that the distributions of stress are similar to those of strain. The high stresses induced in the footwall for the small value of $H/R$ is a noteworthy phenomenon. The maximum stress values are located somewhat closer to the reef plane than the corresponding values of strain.

*Vertical Stress across the Pillar*

For the cases considered in the previous subsection, the induced stresses acting across the pillars were also calculated. The limits of integration in these calculations were

$$r = \sqrt{x^2(\cos^2\phi - 1) + R^2} - x\cos\phi \quad \ldots\ldots\ldots\ldots (27)$$

to $\infty$ and $\phi = 0$ to $2\pi$.

For practical considerations, the corresponding resultant stresses are plotted along a radial line from the centre point of the pillars towards their boundary in Fig. 7. The rapid increase of the resultant vertical stress across the pillar, especially in the case of the small pillar and shallow depth, is obvious from the illustration. The width of boundary zones over which the stresses are very high should be noted. It should, however, be appreciated that the high stresses in this zone are partly due to the assumption introduced earlier that $s_z = s_m$ everywhere in the worked-out area. Since the average convergence just outside the pillar is only a portion of $s_m$, the stresses induced in the perimeter zone of the pillar are expected to be lower than indicated above.

## Design Considerations

The determination of the dimensions of a shaft pillar is governed by a number of well-defined principles. These principles were formulated on the basis of both rock-mechanics and practical-mining considerations. So that they can be utilized in the present study, a brief account of the relevant points is given in this section. The principles are then applied to the design of shaft pillars at shallow and moderate depths.

*Principles of Design*

The first principle concerns the degree of protection required. It can be stated as follows: the magnitudes of all the induced differential movement components and the resultant stresses should be smaller than the corresponding acceptable values. The magnitudes of these acceptable values are not as well specified as could be expected. Consequently, more reliable data are required if the theory is to be utilized and produce an optimum design.

Axial shortening of a shaft or part of a shaft due to induced vertical strain may adversely affect the shaft lining and the shaft equipment. Damage to vertically aligned steelwork and fittings in a vertical shaft is commonly observed as buckling of guides, king-posts, and pipe columns. A large tilt of a section of the shaft axis can make high-speed winding dangerous or even impossible.

A number of authors have suggested critical figures for the components of differential movement. On the basis of an analysis of damaged and undamaged vertical shafts in the central and east Rand, Wilson[6] came to the tentative conclusion that, at a vertical compressive strain of $2 \times 10^{-4}$, shafts began to show signs of damage. The value for the tolerable level of vertical strain used by Salamon[3] was $1 \times 10^{-3}$. Referring to experience, Wagner[7] recently recorded that the acceptable magnitudes of strain and tilt were of the order of $1 \times 10^{-3}$. Daemen[2] in his investigations used a value, suggested by Mohr, of $1{,}5 \times 10^{-3}$ for the vertical strain considered to be critical.

The observations made by Wilson and More O'Ferrall[8] are generally used in the establishment of a critical stress level. According to those observations, tunnels of normal mine dimensions (10 m$^2$) cannot be kept open if the vertical component of the field stress in the rock through which they pass exceeds two-thirds of its uniaxial compressive strength. Damage to such excavations often begins, and control of the damage becomes costly and difficult, when the field stress is equal to one-quarter and exceeds one-half of the uniaxial compressive strength of the rock, respectively. The maximum stress

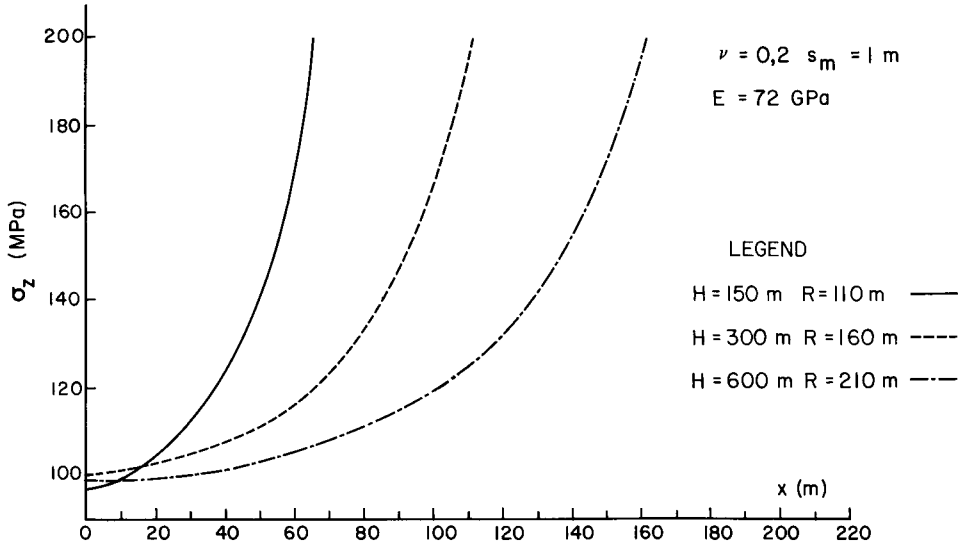


**Fig. 7—Distribution of resultant vertical stress in shaft pillar along a radial line**

value that is tolerable and used for design purposes is referred to as the critical field stress.

The uniaxial compressive strength, for example, of Witwatersrand quartzites is about 220 MPa. It follows that the acceptable magnitude of field stress should be smaller than 110 MPa for the protection of service excavations located in the shaft pillars of South African gold mines, where the horizontal components of virgin stress are one-half of the corresponding vertical component. For a lower value of uniaxial compressive strength, the critical field stress would also be lower.

The second principle relates to the mining layout and states that the design of shaft pillars must be based on the most unfavourable mining layouts, which, under the given conditions, result in the highest possible values of stress and differential-movement components. Adherence to this principle ensures that each critical parameter induced by certain unfavourable mining configurations during some stage of mining is used in the design. It also removes any restrictions as to the layout and sequence of mining outside the shaft pillar.

It will be recalled that, in the present study, the appropriate limits of integration were selected to bring about the most unfavourable mining layouts. Therefore, the most adverse geometries for stress, strain, and tilt were taken into consideration in the preceding sections.

*Stress Considerations*

From a stress point of view, the design involves a determination of the minimum pillar dimension that will bring about an acceptable level of stress along the shaft or in the pillar at the location of important excavations. The most essential of these considerations relates to the magnitude of the vertical resultant stress in the central portion of a pillar, where most of the auxiliary excavations such as pump and hoist chambers, loading stations, and main haulages are located. As already demonstrated, the level of resultant vertical stress at the shaft–reef intersection can be determined. The magnitude and extent of the central portion over which this stress remains more or less constant depend on the dimension of the pillar (Fig. 7).

On the basis of the empirical design criterion used in South African hard-rock mining and described above, the radii of shaft pillars were computed for different critical stresses. From the data derived and by use of a curve-fitting procedure, the curves presented in Fig. 8 were plotted. It was found that the general expression for the radius of a shaft pillar as a function of depth can be written as

$$R = s_m a H^b. \quad \text{.....(28)}$$

The numerical values of the constants a and b for selected critical values of stress within the depth limits of 100 and 1000 m are given in Table II.

TABLE II
NUMERICAL VALUES OF CONSTANTS

| $\sigma_{CR}$ MPa | a | b |
|---|---|---|
| 100 | 13,84 | 0,422 |
| 90 | 10,47 | 0,482 |
| 80 | 6,94 | 0,565 |
| 70 | 3,73 | 0,683 |

At this stage, two observations should be recorded and taken into consideration in the design of a shaft pillar. The fitting of curves to the data is expected, in some depth regions, to result in small divergences from the calculated values. Therefore, an increase of 5 per cent in the radius of the shaft pillar determined by use of either Fig. 8 or equation (28) is recommended.

The second observation is that, for shallow depths, the extent of the central portion over which the critical stresses are constant is relatively small. It is possible that this area is not sufficient to accommodate all the auxiliary excavations. Therefore, before making a final decision, one should determine and plot the variation of the

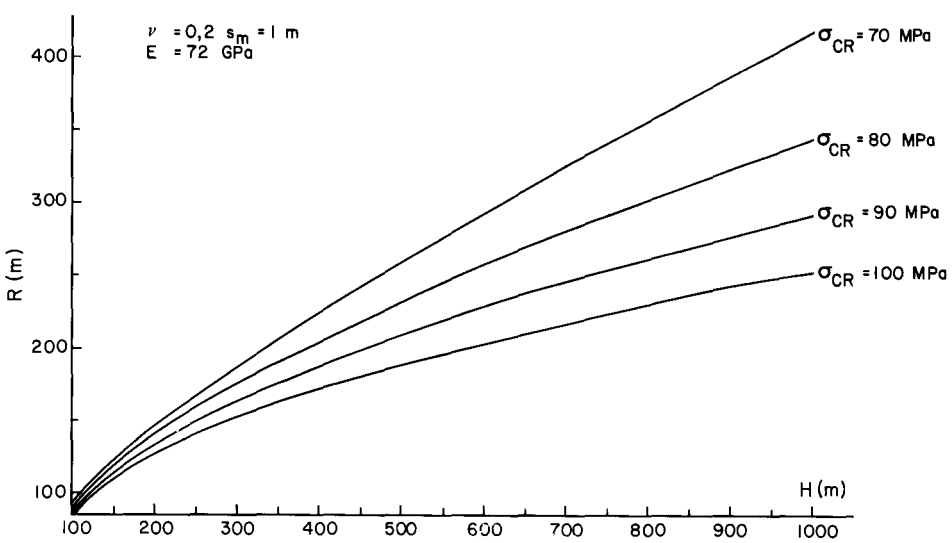


**Fig. 8—Pillar dimensions for different critical stresses**

resultant vertical stress along the radius of shaft pillar selected.

For comparative purposes, the pillar dimensions for both shallow and deep-level mines and for different stoping widths are plotted in Fig. 9 for a critical stress of 100 MPa. It will be seen from this diagram that the effective stoping width has a significant influence on the pillar dimension: a reduction in the effective stoping width results in an appropriate reduction of the pillar radius.

The broken line in Fig. 9 represents the relationship $R = H/2{,}7$. This relationship was derived from observations in coal mines, and is based on the angle-of-draw concept. It is often used in the determination of the size of protective pillars in shallow mines, irrespective of the strength of the rocks involved and the thickness of the mineral deposit extracted. It will be seen that the use of this relationship under the conditions specified in this paper would result in unacceptable pillar sizes.

The values for Figs. 8 and 9 were calculated for a Poisson's ratio of 0,2. Owing to the fact that small changes in this material parameter have a negligible influence on induced stresses and displacements, the data can be used when $\nu$ is within the practical limits of 0,15 and 0,25 without the introduction of any significant errors in the design. It should, however, be noted that the stresses are directly proportional to the modulus of elasticity. This fact has to be borne in mind when the rock is characterized by a substantially different modulus.

Considering the effects of the stresses on the shaft, one comes to the conclusion that they are less important than those across the pillar. In the vertical direction the stress-concentrating effect of the geometry is absent, and the rock is therefore not subjected to stresses as high as in the sidewalls of a horizontal excavation. Furthermore, it can be shown that the horizontal induced stress is very small in comparison with the virgin stresses. Therefore, changes in horizontal field stress will have a negligible effect on the shaft.

As already discussed, the maximum values of vertical stress occur some distance above and below the reef plane. Any horizontal service excavations located near these highly stressed points may be subjected to much higher resultant stresses than those in the centre portion of the pillar. The positioning of auxiliary excavations in the foot- and hangingwalls close to the maximum vertical stresses should therefore be avoided.

*Consideration of Differential Movements*

As indicated earlier, it is essential that the magnitudes of the differential movement components to be brought about by the formation of the shaft pillar should be assessed and controlled in relation to the radius as determined in the preceding subsection. It will be seen from Figs. 3 and 5 that, for the cases studied, the maximum values of both vertical strain and tilt are generally greater than $1 \times 10^{-3}$, which is the acceptable value at present. Therefore, to reduce the maximum differential movement components to tolerable magnitudes, the radius of the shaft pillar would have to be increased.

Fig. 4 can be used in a check on the magnitudes of the maximum components of differential movement. Once the radius of the shaft pillar has been determined by use of the stress criterion, the appropriate maximum values can be found from this graph. A few iterations may be necessary before a decision is taken on the radius of shaft pillar that will satisfy the criteria of both stress and differential movement.

## Summary and Conclusions

The study described in this paper concerned the protection of vertical shafts from the damaging influence of nearby mining in narrow, tabular orebodies in shallow and moderately deep hard-rock mines. The findings of the study were utilized in the design of shaft pillars under the conditions specified.

The distributions of vertical stress and differential movement components along the shaft show that

- for pillars at very shallow depths, the distribution of the above components departs significantly from the trends found for deeper levels;
- at shallow depths, the distributions are asymmetrical about the plane of the deposit;

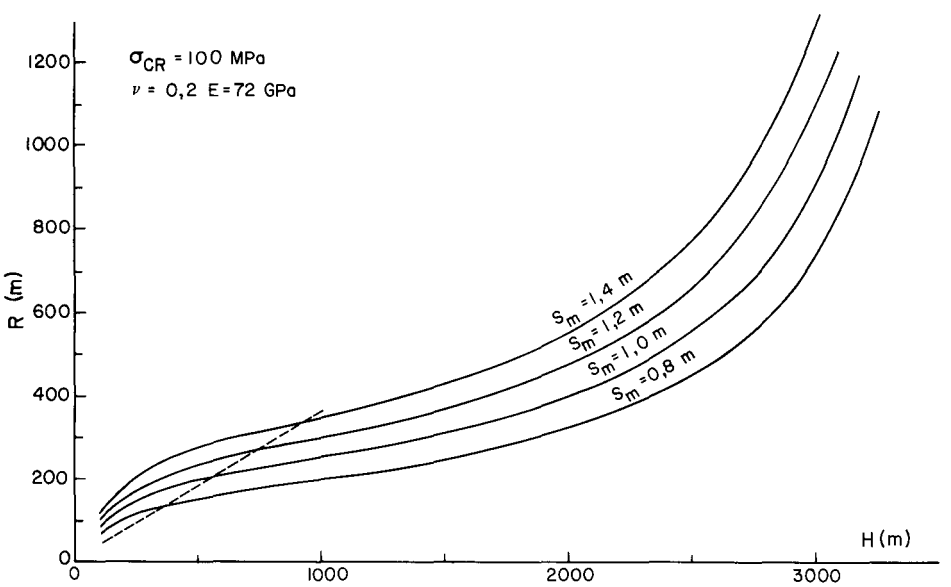


**Fig.9—Pillar dimensions for both shallow and deep-level mines and for different stoping widths**

- with increasing depths, the distribution patterns and the magnitudes of maximum values tend to those established for pillars located at 'infinite depth';
- the maximum values are found at distances between 0,5*R* and 0,6*R* from the reef plane in the foot- and hangingwalls.

While the magnitude of stress depends on both Poisson's ratio and the modulus of elasticity, the components of differential movement depend only on Poisson's ratio.

The distributions of the vertical stress across the pillar indicate that, for small pillars located at shallow depths, the extent of the low-stress central portion is small; in these cases, the selection of pillar dimensions will be governed by the low stress area required for the location of auxiliary excavations.

An important conclusion is that the radius of the shaft pillar is directly proportional to the effective stoping width.

From a practical point of view, the critical importance of the strength of pillar material in determining pillar sizes should be recorded.

Because of possible high values for the maximum components of differential movement in a design, the magnitudes of these components must be determined and compared with the practically acceptable values.


### Acknowledgements

The writer is grateful to Mr R.W. Croeser for the assistance he offered during the preparation of the paper and for the computation of the numerical data. He also gratefully acknowledges that the work presented in the paper was supported financially by the Chamber of Mines of South Africa.


### References


1. SALAMON, M.D.G. Elastic analysis of displacements and stresses induced by the mining of seam or reef deposits. Part III: An application of the elastic theory: Protection of surface installations by underground pillars. *J. S. Afr. Inst. Min. Metall.*, vol. 64. 1964. pp. 468–500.
2. DAEMEN, J.J.K. The effect of protective pillars on the deformation of mine shafts. *Rock Mechanics,* vol. 4, no. 2. 1972. pp. 89–113.
3. SALAMON, M.D.G. Rock mechanics of underground excavations. *Advances in rock mechanics* (Proceedings 3rd Congress of the International Society of Rock Mechanics, Denver, 1974). vol. 1 (B). pp. 951–1099.
4. WAGNER, H., and SALAMON, M.D.G. Strata control techniques in shafts and large excavations. Association of Mine Managers of South Africa, *Papers and Discussions*, 1972–1973. Johannesburg, Chamber of Mines, 1975. pp. 123–138.
5. SALAMON, M.D.G. Elastic analysis of displacements and stresses induced by the mining of seam or reef deposits. Part I: Fundamental principles and basic solutions as derived from idealized models. *J. S.Afr. Inst. Min. Metall.*, vol. 63. 1963. pp. 128–149.
6. WILSON, J.W. The design and support of underground excavations in deep-level, hard-rock mines. PhD thesis, University of the Witwatersrand, 1971.
7. WAGNER, H. Protection of service excavations. *Rock mechanics in mining practice.* Budavari, S. (ed.). Johannesburg, The South African Institute of Mining and Metallurgy, 1983. Chap. 9.
8. WILSON, J.W., and MORE O'FARRALL, R.C. The application of the electrical resistance analogue to mining operations. *J. S.Afr. Inst. Min. Metall.*, vol. 70. 1970. pp. 115–148.


### Addendum

$$u = -\frac{s_m}{8\pi(1-\nu)}\iint_A\left\{\frac{2z(1-2\nu)}{(r^2+z_2^2)^{3/2}}+\frac{z[2(1+\nu)z_1^2-(1-2\nu)r^2]}{(r^2+z_1^2)^{5/2}}+\frac{z[2(1+\nu)z_2^2-(1-2\nu)r^2]}{(r^2+z_2^2)^{5/2}}-\frac{6zz_2(z_1+2\nu H)}{(r^2+z_2^2)^{5/2}}+\frac{6Hz^2(4z_2^2-r^2)}{(r^2+z_2^2)^{7/2}}\right\}r\cos\phi\,\Delta A \quad \text{(A1)}$$

$$v = -\frac{s_m}{8\pi(1-\nu)}\iint_A\left\{\frac{2z(1-2\nu)}{(r^2+z_2^2)^{3/2}}+\frac{z[2(1+\nu)z_1^2-(1-2\nu)r^2]}{(r^2+z_1^2)^{5/2}}+\frac{z[2(1+\nu)z_2^2-(1-2\nu)r^2]}{(r^2+z_2^2)^{5/2}}-\frac{6zz_2(z_1+2\nu H)}{(r^2+z_2^2)^{5/2}}+\frac{6Hz^2(4z_2^2-r^2)}{(r^2+z_2^2)^{7/2}}\right\}r\sin\phi\,\Delta A \quad \text{(A2)}$$

$$w = -\frac{s_m}{8\pi(1-\nu)}\iint_A\left\{\frac{4(1-\nu)z_2}{(r^2+z_2^2)^{3/2}}-\frac{z_1[2(2-\nu)z_1^2+(1-2\nu)r^2]}{(r^2+z_1^2)^{5/2}}-\frac{z_2[2(2-\nu)z_2^2+(1-2\nu)r^2]}{(r^2+z_2^2)^{5/2}}+[z+2H(1-\nu)]\frac{2(2z_2^2-r^2)}{(r^2+z_2^2)^{5/2}}+6Hzz_2\frac{2z_2^2-3r^2}{(r^2+z_2^2)^{7/2}}\right\}\Delta A \quad \text{(A3)}$$

$$\varepsilon_z = -\frac{s_m}{8\pi(1-\nu)} \iint_A \left\{ \frac{4(1-\nu)}{(r^2+z_2^2)^{3/2}} - \frac{12z_2^2(1-\nu)}{(r^2+z_2^2)^{5/2}} + \frac{2(2z_2^2-r^2)}{(r^2+z_2^2)^{5/2}} + \frac{8z_2[z+2H(1-\nu)]}{(r^2+z_2^2)^{5/2}} - \right.$$

$$\frac{6z_1^2(2-\nu)+(1-2\nu)r^2}{(r^2+z_1^2)^{5/2}} - \frac{6z_2^2(2-\nu)+(1-2\nu)r^2}{(r^2+z_2^2)^{5/2}} + \frac{5z_1^2[2z_1^2(2-\nu)+(1-2\nu)r^2]}{(r^2+z_1^2)^{7/2}} +$$

$$\frac{5z_2^2[2z_2^2(2-\nu)+(1-2\nu)r^2]}{(r^2+z_2^2)^{7/2}} - \frac{10z_2(2z_2^2-r^2)[z+2H(1-\nu)]}{(r^2+z_2^2)^{7/2}} + \frac{6H[z_2(2z_2^2-3r^2)+3z(2z_2^2-r^2)]}{(r^2+z_2^2)^{7/2}} -$$

$$\left. \frac{42Hzz_2^2(2z_2^2-3r^2)}{(r^2+z_2^2)^{9/2}} \right\} \Delta A \quad \ldots\ldots\ldots\ldots\ldots\ldots\ldots\ldots\ldots\ldots\ldots\ldots \quad \text{(A4)}$$

$$t_x = -\frac{s_m}{8\pi(1-\nu)} \iint_A \left\{ \frac{4z_1(1+\nu)}{(r^2+z_1^2)^{5/2}} - \frac{8z_2(1-2\nu)+6(z_1+2\nu H)}{(r^2+z_2^2)^{5/2}} - \frac{5z_1[2z_1^2(1+\nu)-(1-2\nu)r^2]}{(r^2+z_1^2)^{7/2}} - \right.$$

$$\frac{5z_2[2z_2^2(1+\nu)-(1-2\nu)r^2]}{(r^2+z_2^2)^{7/2}} + \frac{30z_2^2(z_1+2\nu H)}{(r^2+z_2^2)^{7/2}} + \frac{6H(8zz_2+4z_2^2-r^2)}{(r^2+z_2^2)^{7/2}} -$$

$$\left. \frac{42zz_2H(4z_2^2-r^2)}{(r^2+z_2^2)^{9/2}} \right\} r\cos\phi\ \Delta A \quad \ldots\ldots\ldots\ldots\ldots\ldots\ldots\ldots\ldots\ldots\ldots\ldots \quad \text{(A5)}$$

$$\sigma_z = \frac{2\nu E s_m}{8\pi(1-\nu^2)(1-2\nu)} \iint_A \left\{ \frac{2(1-2\nu)}{(r^2+z_2^2)^{3/2}} - \frac{(1-2\nu)r^2}{(r^2+z_1^2)^{5/2}} - \frac{4(1-2\nu)r^2}{(r^2+z_2^2)^{5/2}} - \frac{6z_2(z_1+2\nu H)}{(r^2+z_2^2)^{5/2}} + \right.$$

$$\frac{2(1+\nu)z_1^2-(1-2\nu)r^2}{(r^2+z_1^2)^{5/2}} + \frac{2(1+\nu)z_2^2-(1-2\nu)r^2}{(r^2+z_2^2)^{5/2}} + \frac{12Hz(2z_2^2-r^2)}{(r^2+z_2^2)^{7/2}} + \frac{15z_2(z_1+2\nu H)r^2}{(r^2+z_2^2)^{7/2}} -$$

$$\left. \frac{5[2(1+\nu)z_1^2-(1-2\nu)r^2]r^2}{2(r^2+z_1^2)^{7/2}} - \frac{5[2(1+\nu)z_2^2-(1-2\nu)r^2]r^2}{2(r^2+z_2^2)^{7/2}} - \frac{21Hz(4z_2^2-r^2)r^2}{(r^2+z_2^2)^{9/2}} \right\} \Delta A -$$

$$\frac{E s_m}{8\pi(1+\nu)(1-2\nu)} \iint_A \left\{ \frac{4(1-\nu)}{(r^2+z_2^2)^{3/2}} - \frac{12z_2^2(1-\nu)}{(r^2+z_2^2)^{5/2}} + \frac{2(2z_2^2-r^2)}{(r^2+z_2^2)^{5/2}} + \frac{8z_2[z+2H(1-\nu)]}{(r^2+z_2^2)^{5/2}} - \right.$$

$$\frac{6z_1^2(2-\nu)+(1-2\nu)r^2}{(r^2+z_1^2)^{5/2}} - \frac{6z_2^2(2-\nu)+(1-2\nu)r^2}{(r^2+z_2^2)^{5/2}} + \frac{5z_1^2[2z_1^2(2-\nu)+(1-2\nu)r^2]}{(r^2+z_1^2)^{7/2}} +$$

$$\frac{5z_2^2[2z_2^2(2-\nu)+(1-2\nu)r^2]}{(r^2+z_2^2)^{7/2}} - \frac{10z_2(2z_2^2-r^2)[z+2H(1-\nu)]}{(r^2+z_2^2)^{7/2}} + \frac{6H[z_2(2z_2^2-3r^2)+3z(2z_2^2-r^2)]}{(r^2+z_2^2)^{7/2}} -$$

$$\left. \frac{42Hzz_2^2(2z_2^2-3r^2)}{(r^2+z_2^2)^{9/2}} \right\} \Delta A \quad \ldots\ldots\ldots\ldots\ldots\ldots\ldots\ldots\ldots\ldots\ldots\ldots \quad \text{(A6)}$$